applied sciences

MDPI

Article

Creep Mechanical Properties of Marble Under Graded Unloading Conditions

Yongcheng Guo [1,2,*], Zhuo Yu [1], Shunan Wang [1], Jianlin Li [1,2] and Huafeng Deng [1,2]

[1] Key Laboratory of Geological Hazards in Three Gorges Reservoir Area, Ministry of Education, China Three Gorges University, Yichang 443002, China; 202308140021044@ctgu.edu.cn (Z.Y.)
[2] Key Laboratory of Disaster Prevention and Mitigation, China Three Gorges University, Yichang 443002, China
* Correspondence: gyc@ctgu.edu.cn

Abstract

To study the creep mechanical behavior of surrounding rock under the coupled effect of confining pressure unloading and deviatoric stress increase during the excavation of deep underground engineering, triaxial creep tests under stepwise unloading of confining pressure and loading of deviatoric stress were conducted using marble as the research object. The influences of different initial confining pressures, unloading amounts, and stress levels on the axial and circumferential creep deformation, creep rate, and failure characteristics of marble were systematically analyzed. The results indicate the following: (1) As the amount of confining pressure unloading increases, the creep failure stress of marble decreases significantly, and the test duration is markedly shortened. (2) Under conditions of small unloading amounts, the creep rate initially decreases and then increases with increasing stress levels, while under large unloading amounts, the creep rate monotonically increases with stress levels, indicating that confining pressure unloading significantly weakens the stability of the rock mass during creep. (3) Based on the test results, a three-dimensional non-stationary Nishihara creep model suitable for the stress path of stepwise confining pressure unloading and deviatoric stress loading was established. The model calculations agree well with the experimental data, effectively describing the entire creep process of marble under unloading conditions. The research findings can provide a reference for the long-term stability analysis of the surrounding rock after excavation in deep underground engineering.

Keywords: marble; unloading creep; confining pressure unloading; creep rate; long-term strength

Check for updates

Academic Editor: Tiago Filipe da Silva Miranda

Received: 6 February 2026
Revised: 13 March 2026
Accepted: 21 March 2026
Published: 29 March 2026

Copyright: © 2026 by the authors. Licensee MDPI, Basel, Switzerland. This article is an open access article distributed under the terms and conditions of the Creative Commons Attribution (CC BY) license.

1. Introduction

As the shallow resources become increasingly depleted and the scope of human activities expands, more and more underground projects are moving towards the deeper layers [1–3]. During the excavation of underground projects that are deeply buried, the original stress balance of the surrounding rock is disrupted. The surrounding pressure continues to decrease, and the deviatoric stress gradually accumulates. The stress state of the surrounding rock evolves continuously in time and space as the excavation progresses, which is highly likely to trigger significant time-dependent deformations and long-term stability issues [4–6]. Therefore, conducting systematic research on the mechanical behavior of the surrounding rock caused by excavation of underground projects buried deep underground is of great significance for revealing the long-term deformation mechanism of the surrounding rock and ensuring the safety of the projects.

Regarding the instantaneous and time-dependent mechanical properties of rocks, a large number of experimental studies have been conducted by scholars both at home and abroad [7–9]. In terms of uniaxial creep tests, Zhao Yue et al. [10] conducted uniaxial compression and creep tests on marble in different chemical environments and freeze–thaw cycles, and systematically evaluated the influence of environmental factors on the long-term strength of marble; Mishra et al. [11] and Zhao Na et al. [12] revealed the evolution process of rock creep failure from the perspectives of time deformation and macro-microscopic evolution; and Li Ziyi et al. [13] and Guo Yongcheng et al. [14], starting from dry-wet cycling and water pressure conditions respectively, analyzed the influence patterns of environmental factors and stress levels on the long-term mechanical properties of rocks.

Regarding the aspect of triaxial creep tests, Hu Minyun et al. [15] studied the triaxial shear creep characteristics of over-consolidated saturated clay and established a corresponding model; Shi Weizheng et al. [16] and Zhou Ruihete et al. [17] conducted graded unloading creep tests on soft rocks and siltstones and analyzed the effects of confining pressure unloading on creep deformation and long-term strength. Yan Zijian et al. [18] conducted a constant axial pressure graded unloading of confining pressure creep test on Jinping dolomite and pointed out that the level of deviatoric stress is an important factor affecting the creep deformation of the rock. Furthermore, Ni Jing et al. [19], Liu Xinxi et al. [20], Guo Xiafei et al. [21], and others also conducted systematic studies on the triaxial creep characteristics of different rock and soil materials from the perspectives of confining pressure levels, loading methods, and freeze–thaw effects.

Overall, existing studies have conducted in-depth analyses of the time-dependent mechanical behavior of rocks based on aspects such as uniaxial creep, triaxial constant load creep, and staged unloading of confining pressure creep. However, there are still some limitations: on the one hand, earlier studies mostly focused on single stress paths such as constant axial pressure with staged confining pressure removal or constant confining pressure with axial pressure addition; on the other hand, although staged unloading of confining pressure or increasing axial pressure have been gradually introduced in recent years, most studies still have not fully considered the typical and crucial stress path feature of staged confining pressure removal and synchronous increase in deviatoric stress during the excavation of deep underground engineering. The above research fails to comprehensively reflect the dynamic coupling effect of the stress paths of the surrounding rock under actual excavation conditions, which restricts the in-depth understanding of the long-term creep deformation and stability issues of the surrounding rock.

In view of this, this paper takes marble as its research object and designs and conducts triaxial creep tests under the path of graded unloading of confining pressure and loading. It systematically analyzes the influence laws of confining pressure unloading amount, initial confining pressure, and time on the creep deformation and deformation rate of marble, and further establishes a creep constitutive model applicable to this stress path. The research results contribute to a deeper understanding of the creep behavior of rocks under unloading conditions and have certain engineering reference value for the long-term stability analysis of surrounding rocks in deep underground engineering.

2. Materials and Methods

2.1. Sample Preparation and Test Equipment

The marble material used in this test was taken from a certain area in southwest China. Large blocks of rock with uniform texture and color were selected and made into standard cylindrical samples of $\Phi 50 \times 100$ mm in accordance with the requirements of the "Standard Test Methods for Engineering Rock Mass" [22], as shown in Figure 1. To ensure the reliability of the test results, the samples were initially screened by the weighing

method to eliminate those with significant density deviations. Then, the longitudinal wave velocity of the samples was measured using the ZBL-U510 ultrasonic testing instrument to strictly select samples with similar wave velocities for the subsequent tests. After the initial screening, the density range of the rock samples was 2.820–2.840 g/cm^3, and the shear wave velocity was 2.950–3.100 km/s. To minimize the influence of thermal fluctuations on the long-term creep measurements, the ambient temperature in the laboratory was maintained constant at 20 ± 0.5 °C throughout all tests.



Figure 1. Marble rock sample.

2.2. Experimental Protocol Design

The experiment was conducted using the TOP INDUSTRIE fully automatic rock triaxial rheometer (as shown in Figure 2), and involved sequential execution of conventional triaxial loading tests, triaxial unloading tests, and graded unloading of confining pressure, followed by axial loading creep tests.

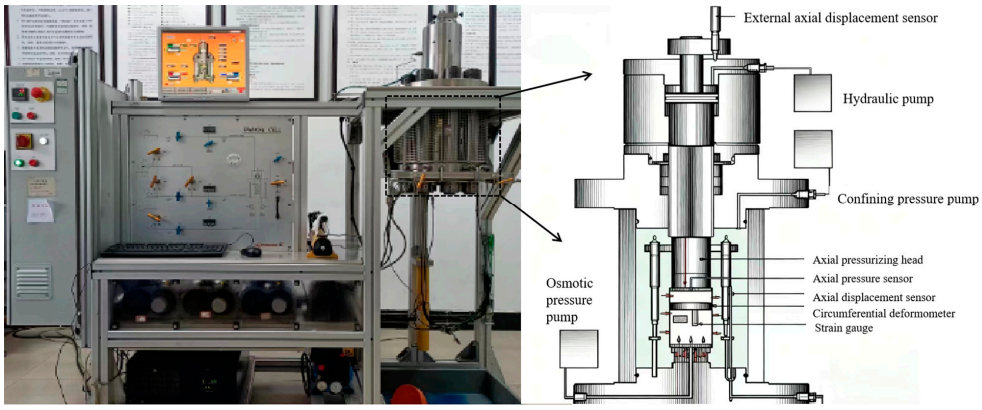


Figure 2. TOP INDUSTRIE Triaxial Rheometer.

(1) Conventional triaxial loading test

To obtain the peak strength of marble under different confining pressures, a stress-controlled method was employed. The confining pressure was applied at a loading rate of 1.5 MPa/min to 0, 5, 10, 15 and 20 MPa, and then the axial stress was continuously applied until the specimen broke. The peak strengths under confining pressure were 85.22, 149.99, 188.48, 210.27 and 230.91 MPa, respectively, providing a basis for the selection of confining stress levels in subsequent unloading tests and creep tests.

(2) Triaxial unloading test

During the excavation process of deep underground engineering, the surrounding rock can be approximately regarded as having relatively small axial stress changes within a certain range, while the circumferential stress rapidly decreases as the excavation progresses.

Based on this engineering characteristic, the test method of removing confining pressure under constant axial pressure was adopted to study the failure behavior of marble during the process of confining pressure removal.

In the unloading test, 80% of the peak deviatoric stress corresponding to the specified confining pressure was selected as the deviatoric stress level during unloading. This stress level lies between the splitting strength ratio of marble (0.67–0.77) and the damage strength ratio (0.84–0.96). The interior of the sample has already undergone stable crack propagation and entered the plastic deformation stage, which is conducive to inducing instability failure during the unloading of confining pressure, and at the same time ensures the comparability of the test results under different confining pressure conditions.

The specific steps are as follows: Load the confining pressure at a rate of 1.5 MPa/min to 5, 10, 15 and 20 MPa, respectively. Then, apply axial pressure to make the deviatoric stress reach 80% of the corresponding peak strength and keep it constant. Finally, gradually unload the confining pressure at a rate of 1.5 MPa/min until the specimen fails. The corresponding unloading failure confining pressures are 0.80, 3.02, 6.07 and 8.01 MPa, and the unloading amounts are 4.20, 6.98, 8.93 and 11.99 MPa, respectively.

(3) Graded unloading confining pressure and deviatoric stress creep test

To simulate the stress path characteristics of gradually reducing confining pressure and synchronous increase in deviatoric stress during the excavation of deep underground projects, a series of creep tests with stepwise reduction in confining pressure and simultaneous application of deviatoric stress were conducted. The influence of initial confining pressure, unloading path, and deviatoric stress level on the creep characteristics of marble was focused on.

The selection of the confining pressure unloading amount adopts two schemes:

Scheme 1: Based on the unloading amount obtained from the triaxial unloading test, take 25% of it as the unloading amount for a single stage of confining pressure, corresponding to 1.05, 1.75, 2.23, and 3.00 MPa, respectively. The aim is to obtain the same confining pressure unloading ratio of marble creep responses under different initial confining pressures, and to achieve a normalized comparative analysis [23].

Option 2: Determine different levels of staged unloading directly based on the confining pressure (as shown in Table 1), to analyze the effects of different unloading amplitudes on the creep deformation and failure mode under the same initial confining pressure.

Table 1. Confining pressure graded unloading.

Initial Confining Pressure/MPa	Unloading Magnitude per Step/MPa	Incremental Deviator Stress
5	0.5, 2, 3	10% of the initial peak compressive stress
10	1, 3, 4	
15	1, 3, 5	
20	2, 4, 5	

The test procedure for the stepwise unloading and loading creep test is as follows:

1. Apply confining pressure (σ_3) to the target initial value (e.g., 15 MPa) at a constant rate.
2. Increase axial stress (σ_1) to achieve an initial deviatoric stress ($q = \sigma_1 - \sigma_3$) equal to 40% of the peak deviatoric stress under the initial confining pressure. Hold this state constant for 24 h to observe creep.
3. Reduce σ_3 by a predetermined amount (e.g., 1 MPa) at a constant rate (1.5 MPa/min). Note that σ_1 is kept constant during this phase.

4. After the confining pressure reduction is complete, immediately increase σ_1 to raise the deviatoric stress by an additional 10% of the initial peak deviatoric stress. Hold this new state constant for another 24 h.

   Repeat steps 3 and 4 until the specimen fails.

3. Analysis of the Creep Characteristics of Marble Under Stepwise Unloading

3.1. Evolutionary Characteristics of Creep Deformation

Figure 3 presents the entire process curves of the creep strain over time for different graded unloading amounts under an initial confining pressure of 15 MPa. It can be observed that under the combined effect of graded unloading of confining pressure and applied deviatoric stress, the creep process of marble generally undergoes three typical stages: attenuation creep, steady-state creep, and accelerated creep. However, the duration and evolution characteristics of each stage are significantly influenced by the unloading amount.

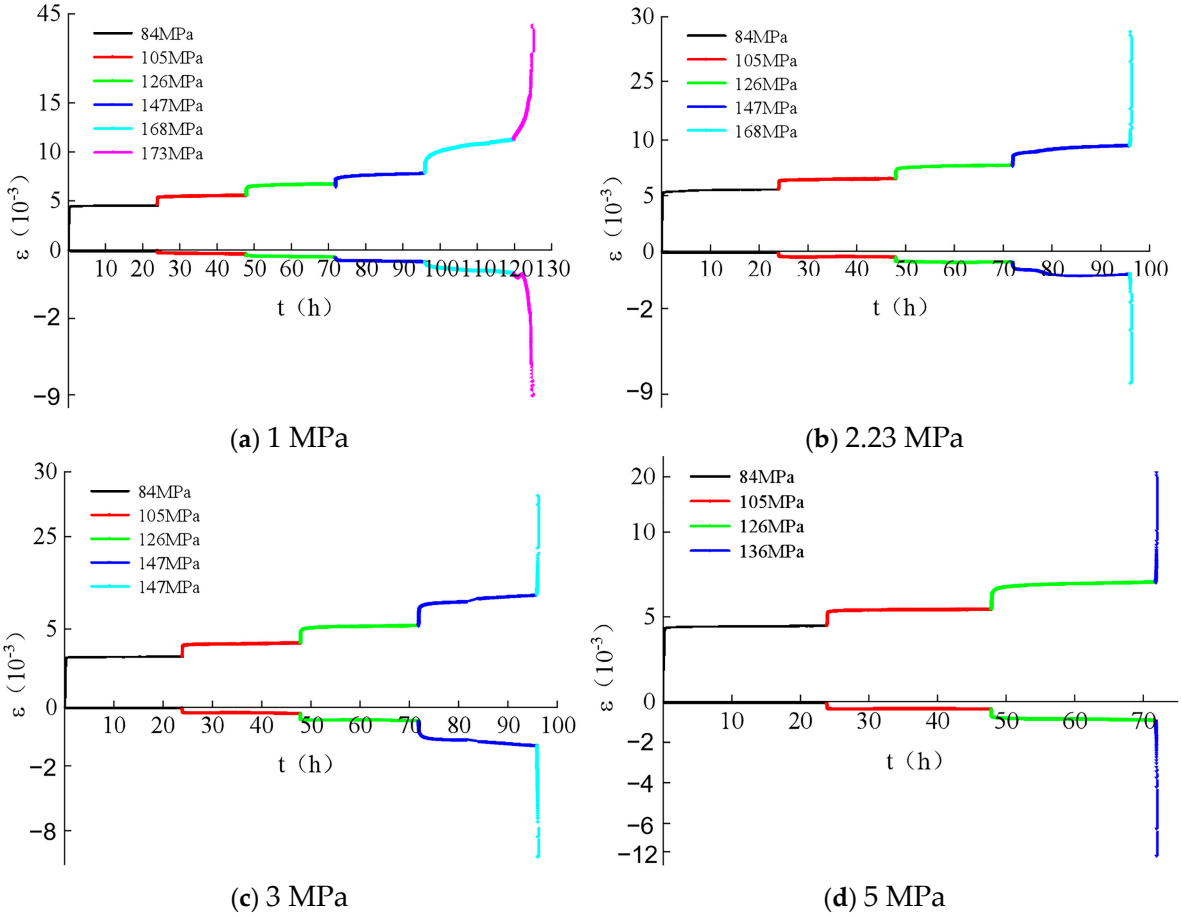


Figure 3. Creep strain–time relationship curves for initial confining pressure of 15 MPa.

When the graded unloading amount is relatively small (1 MPa), the specimen mainly exhibits attenuated creep and steady-state creep in the first five stress levels. The sixth stress level reaches the failure stress level, and the specimen gradually enters the accelerated creep stage after steady-state creep and eventually fails. As the staged unloading pressure increased to 2.23 MPa and 3 MPa, the stress level at which the specimen failed was advanced to the fifth level; when the unloading pressure further increased to 5 MPa, the stress level at failure was advanced to the fourth level, and the duration of the accelerated creep stage was extremely short. After the loading of the deviatoric stress was completed, the specimen rapidly underwent instability failure.

The total test durations of the specimens under different unloading quantities were 124.74 h, 96.08 h, 96.19 h and 72.13 h, respectively, and the corresponding failure stresses were 173 MPa, 165.62 MPa, 147 MPa and 136 MPa. Figure 4 further demonstrates that under the same initial confining pressure conditions, as the amount of confining pressure reduction increases, the creep failure stress significantly decreases, and the total test duration is significantly shortened. This indicates that a larger amount of confining pressure reduction significantly weakens the deformation stability of marble during the long-term loading process.

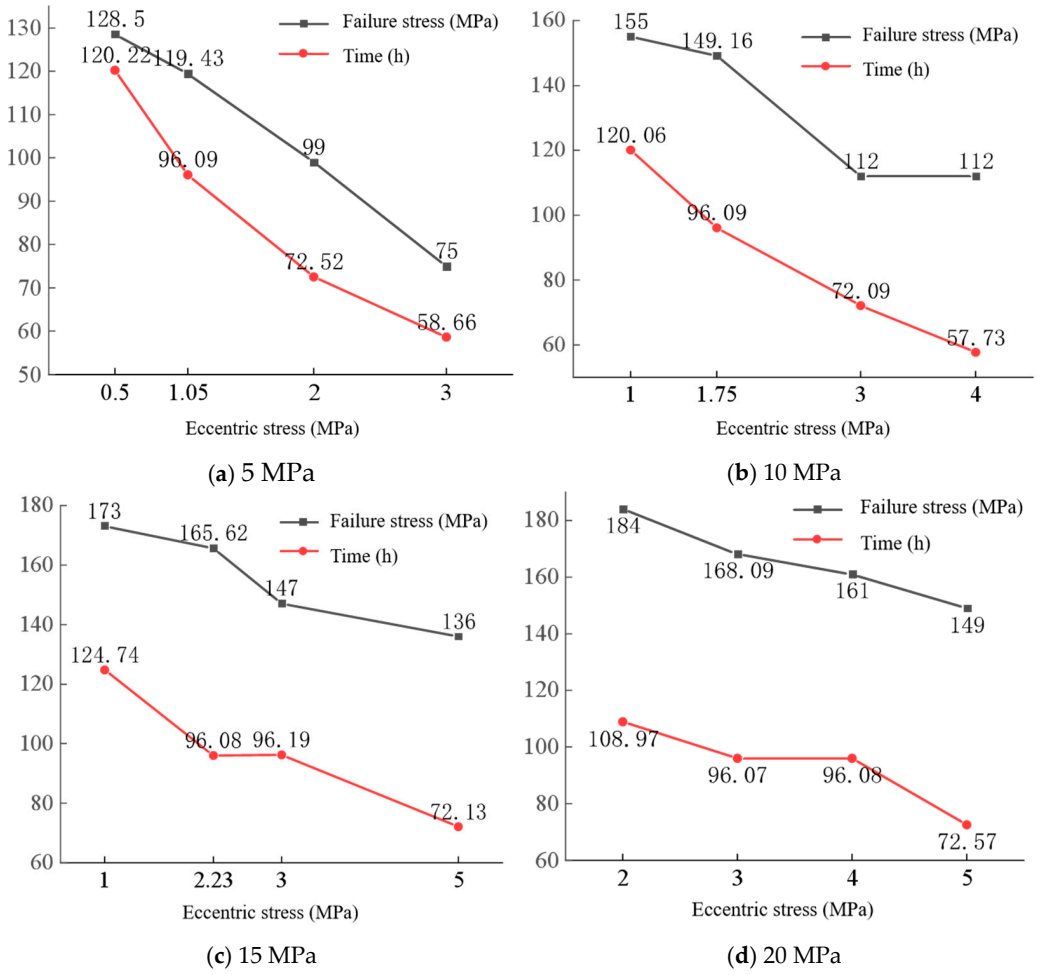


Figure 4. Creep test: destructive stress test duration under different confining pressures.

3.2. Analysis of Creep Rate Characteristics and Mechanism

Figure 5 shows the evolution laws of the axial and circumferential creep rates of the specimens under different unloading amounts under the initial confining pressure of 15 MPa. In general, both the axial and circumferential creep rates increase with the increase in stress level, and a sudden increase occurs when approaching the failure stress level. The most important trend to observe in Figure 5 is the effect of unloading magnitude on creep acceleration. As the unloading magnitude increases from 1 MPa (panel a) to 5 MPa (panel d), the creep rate at equivalent stress levels rises substantially, and the onset of rapid acceleration (marking the transition to tertiary creep) occurs at progressively lower stress levels. For example, under 5 MPa unloading, the creep rate at the fourth stress level is an order of magnitude higher than under 1 MPa unloading, indicating that larger unloading steps significantly accelerate failure.

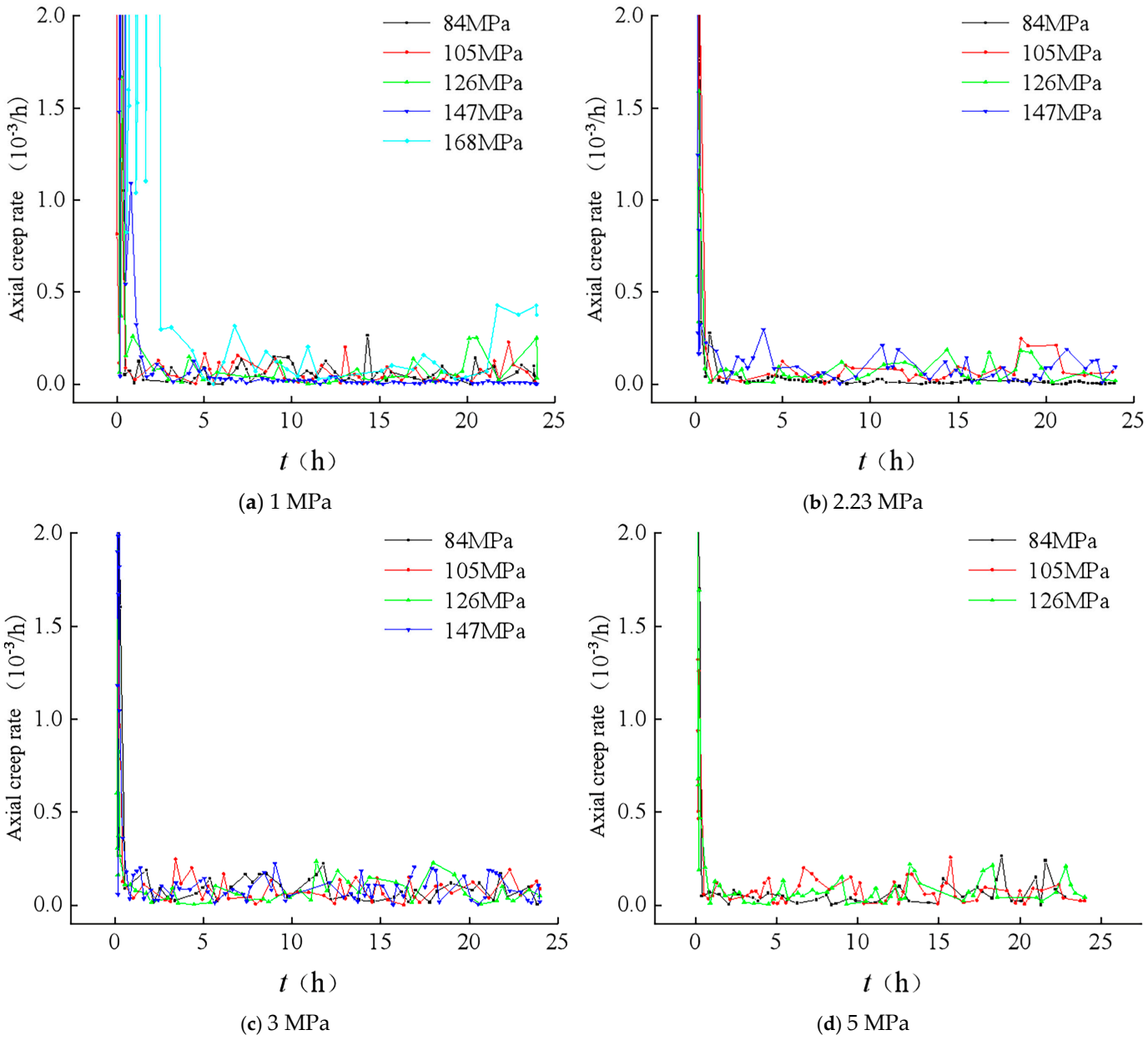
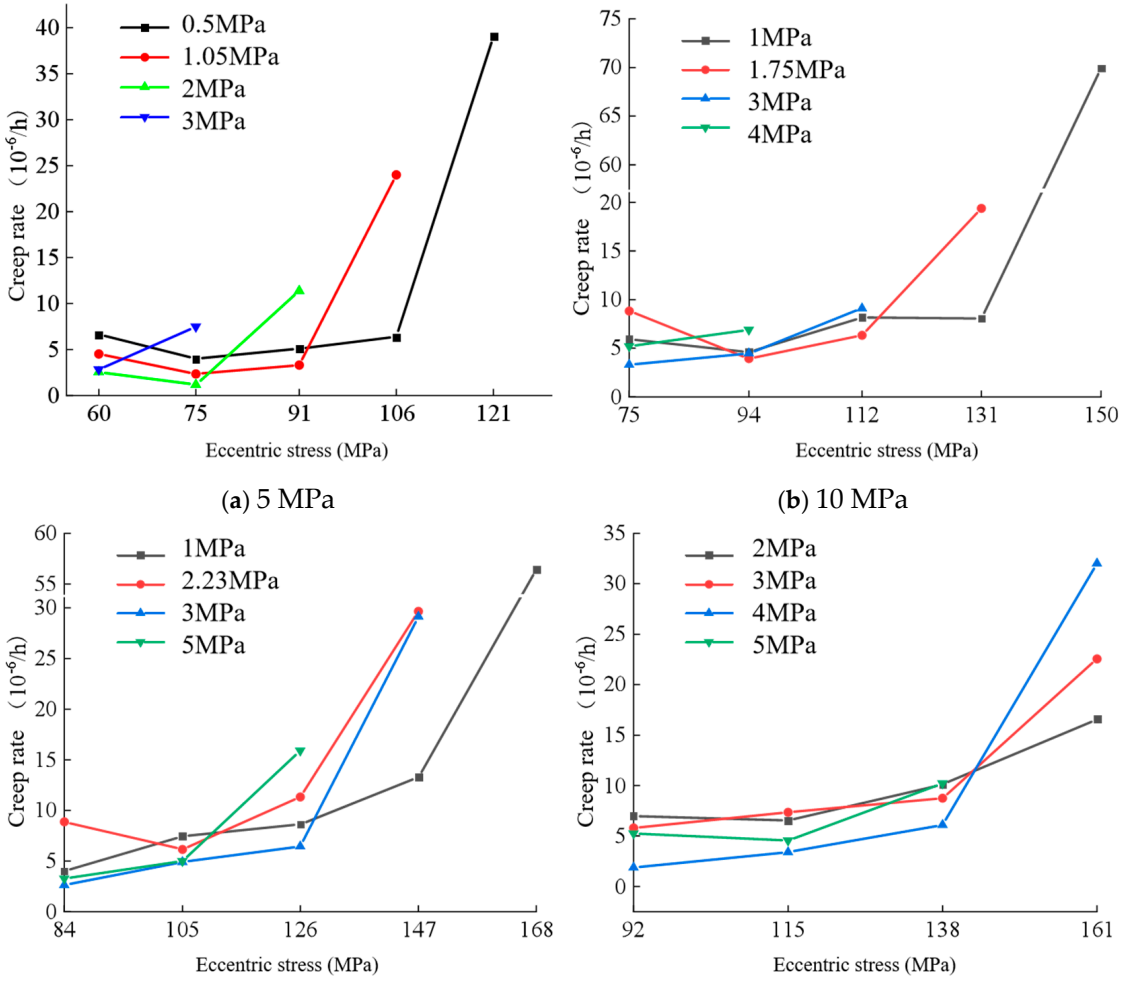


Figure 5. Axial creep rates for various unloading stages under 15 MPa initial confining pressure.

By comparing different unloading amounts, it can be observed that in the samples subjected to a graded unloading at 3 MPa and 5 MPa, the axial creep rate at the fourth stress level is 4.51 times and 3.19 times that of the third stress level, respectively, while the circumferential creep rate increases by 10.39 times and 15.41 times. This indicates that at the quasi-damage stress level, the circumferential creep rate is more sensitive to unloading disturbances, and this sensitivity significantly increases with the increase in unloading amount.

Further analysis of the axial creep rate under different initial confining pressures (Figure 6) reveals that when the unloading amount is relatively small, the axial creep rate of the same sample shows a changing pattern of first decreasing and then increasing with the increase in stress level; while when the unloading amount is large, this trend shifts to a monotonic increase with the stress level. This phenomenon indicates that under small unloading conditions, the confining pressure can still provide certain constraints for the closure of fractures and the stability of the structure. The initial increase in deviatoric stress mainly causes the compaction of fractures and the adjustment of the structure, with

a brief decrease in the creep rate; as the stress further increases, the fractures reopen and expand, and the creep rate subsequently increases. In contrast, under the condition of large unloading, the rapid attenuation of confining pressure weakens the closure effect of fractures, causing fracture expansion to take the dominant position from the initial stage, and the creep rate continues to increase with the stress level.



(**a**) 5 MPa (**b**) 10 MPa

(**c**) 15 MPa (**d**) 20 MPa

Figure 6. Axial creep rates at various initial confining pressures.

3.3. Analysis of Deformation Characteristics Comparison

(1) Comparison of different unloading amounts under the same initial confining pressure

The deformation of the sample is decomposed into the instantaneous strain during the stress adjustment stage and the creep strain during the constant pressure stabilization stage. Figure 7 shows the distribution characteristics of the deformation components under different unloading conditions at an initial confining pressure of 15 MPa. The results indicate that before the deviatoric stress reaches the damage strength, the axial instantaneous strain varies little under different stress levels, and it is mainly controlled by the deviatoric stress increment, while the circumferential instantaneous strain is more sensitive to the change in confining pressure and shows a significant increasing trend as the unloading amount increases. In this study, "instantaneous strain" is defined as the time-independent deformation recorded immediately upon each stress adjustment (within seconds), which includes both elastic and instantaneous plastic components.

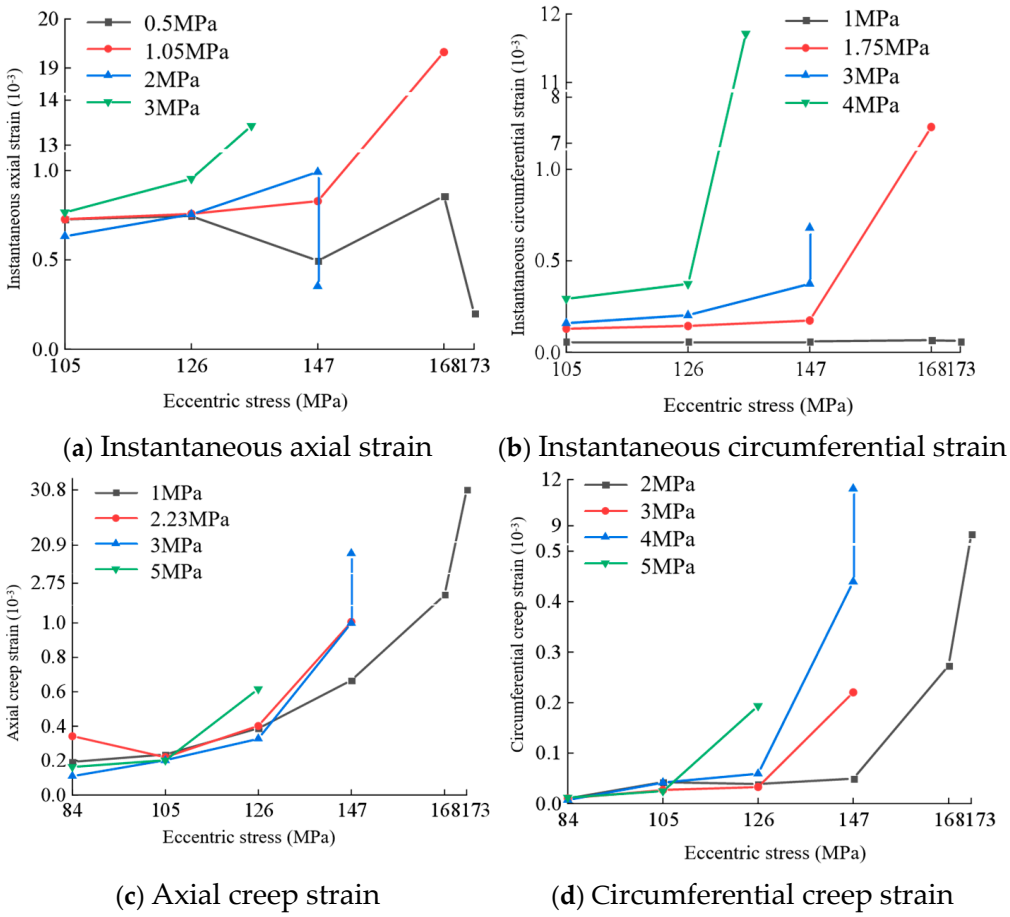


Figure 7. Instantaneous strain and creep strain for each stress level under 15 MPa confining pressure.

In terms of creep deformation, under conditions of larger unloading, both axial and circumferential creep strains continuously increase with the stress level. However, under conditions of smaller unloading, the initial strain shows certain fluctuations, and then gradually transforms into an increasing trend, indicating that the magnitude of confining pressure unloading has a significant regulatory effect on the cumulative process of creep.

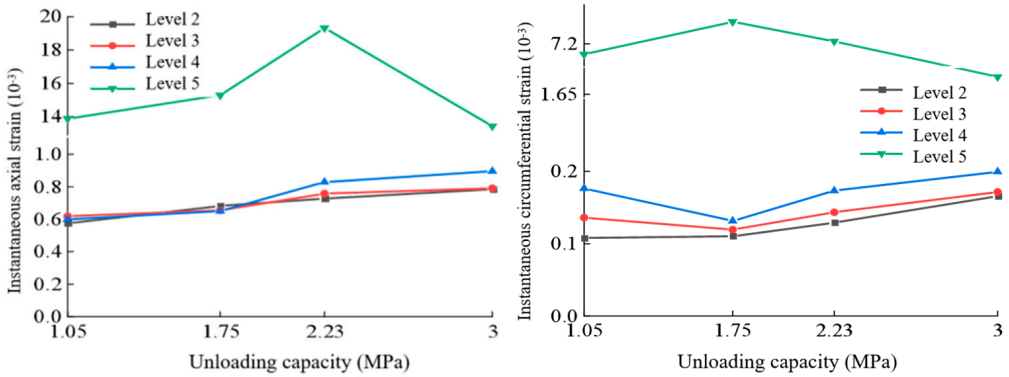
(2) Comparison under the same unloading ratio condition at different initial confining pressures

Figures 8 and 9 illustrate the instantaneous deformation and creep deformation patterns of each stress level under different initial confining pressures and the same unloading ratio. The results show that as the initial confining pressure increases, the overall instantaneous axial strain of each level increases, while the instantaneous circumferential strain shows non-monotonic changes under different stress levels. For creep deformation, under the third to fourth stress levels, the circumferential creep strain decreases with the increase in the initial confining pressure. This is mainly attributed to the fact that after multiple unloading of the confining pressure, the high initial confining pressure samples still maintain a relatively high residual confining pressure, which has a stronger inhibitory effect on the circumferential deformation.

(3) Comparison under the same unloading amount condition under different initial confining pressures

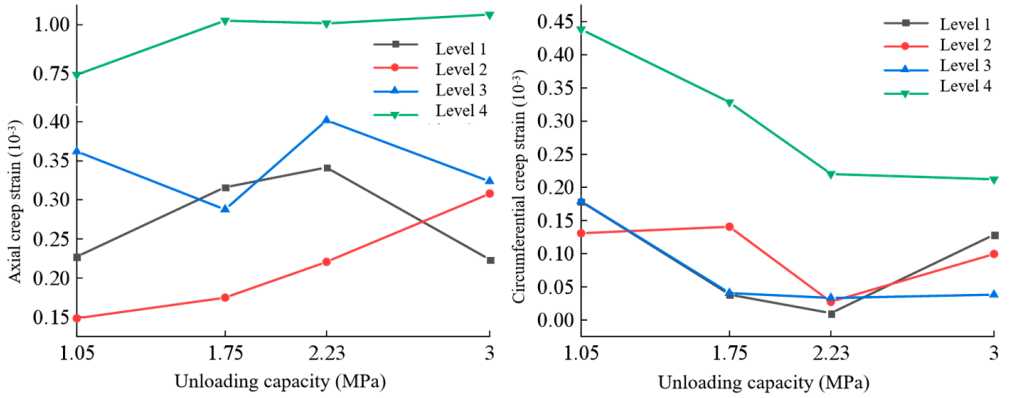
Under the same unloading load (3 MPa) conditions (Figures 10 and 11), the instantaneous strain and creep strain of the samples with different initial confinements generally showed an increasing trend as the stress level increased. During the low stress level stage,

the deformation differences among the samples were relatively small; however, near the failure stress level, the increment in creep strain significantly increased, indicating that the creep accumulation before failure played a crucial role in promoting the instability process.



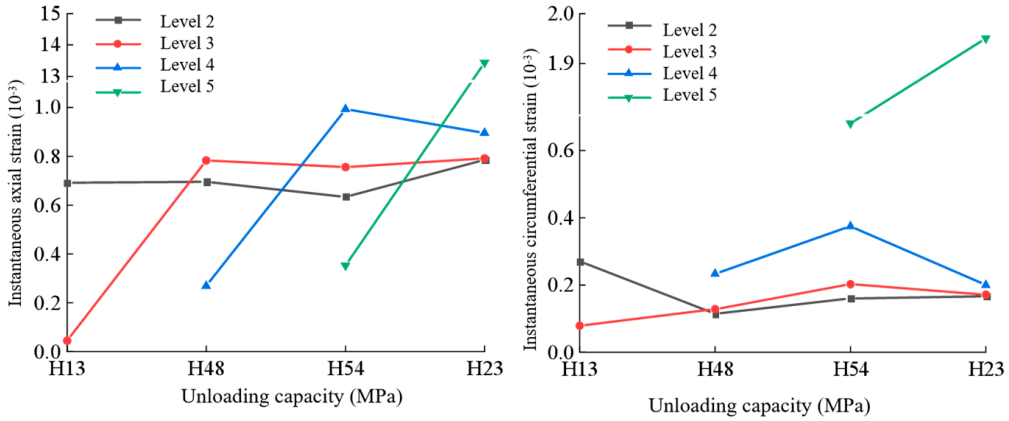
(**a**) Axial (**b**) Circumferential

Figure 8. Instantaneous deformation of each grade for the same unloading ratio test with different initial confining pressures.



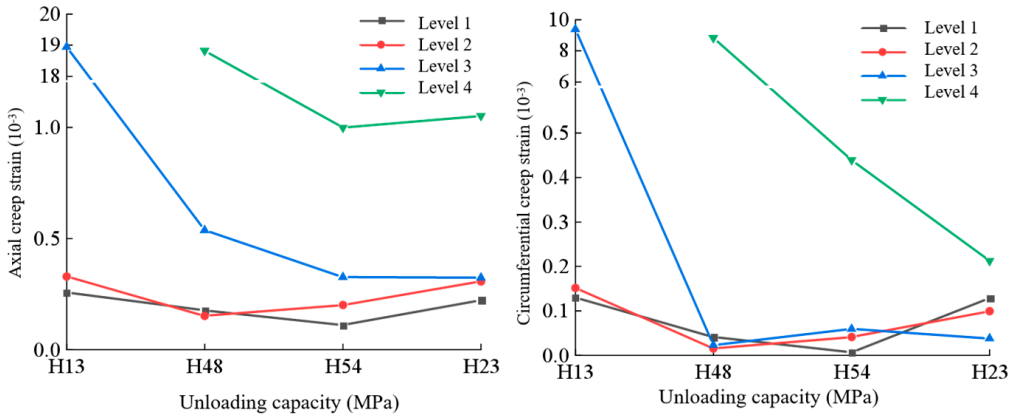
(**a**) Axial (**b**) Circumferential

Figure 9. Creep deformation of each grade for the same unloading ratio test with different initial confining pressures.



(**a**) Axial (**b**) Circumferential

Figure 10. Stage-wise instantaneous deformation under different initial confining pressures with identical unloading magnitude.



(**a**) Axial (**b**) Circumferential

Figure 11. Step-wise creep deformation under different initial confining pressures with identical unloading magnitude.

3.4. Long-Term Intensity Characteristics

The long-term strength of marble was determined using the isochronous stress–strain curve method. For each isochronous curve (plotted at specific time intervals), the turning point where the curve deviates from linearity was identified. To minimize subjectivity, we employed a quantitative criterion: the turning point was defined as the stress level at which the local secant modulus of the isochronous curve decreased to 85% of the initial tangent modulus (representing a 15% deviation from linearity). This threshold was selected based on the observation that beyond this point, the curves exhibited progressive nonlinearity leading to failure. Although this method involves a degree of empirical judgment, it is a widely accepted approach in rock mechanics for estimating long-term strength [24]. The determined values are presented in Table 2.

Table 2. Long-term strength of creep specimens with different initial confining pressures.

Initial Confining Pressure (MPa)	Long-Term Intensity (MPa)	Failure Strength (MPa)	Ratio
0	66.23	77	0.86
	87.21	119.43	0.73
5	75.94	99	0.77
	63.24	75	0.84
	113.84	149.16	0.76
10	96.06	112	0.86
	92.89	112	0.83
	122.39	165.62	0.74
15	116.23	147	0.79
	108.13	136	0.80
	141.20	184	0.77
20	135.07	168.09	0.80
	116.86	149	0.78

The results show that the ratio of long-term strength to failure strength is the highest under uniaxial conditions; as the initial confining pressure increases and the unloading amount increases, this ratio generally shows a decreasing trend. From this, it can be inferred that the confining pressure has a significant inhibitory effect on time-dependent failure. Under high confining pressure conditions, the rock's ductility increases, the slow expansion process of microcracks is restricted, and the failure mode gradually shifts from creep dominance to stress-controlled shear failure. In addition, a large unloading amount

leads to a sudden drop in confining pressure, causing rapid release of elastic strain energy and accelerated penetration of fractures, weakening the dominant role of creep in the failure process, and making the long-term strength closer to the instantaneous failure strength.

3.5. The Failure Characteristics of Marble Under Staged Unloading Conditions

The typical failure patterns of the specimens under different initial confining pressures and unloading amounts are shown in Figure 12. The numbers in the brackets in the figure names represent the graded unloading amounts, with the unit being MPa.

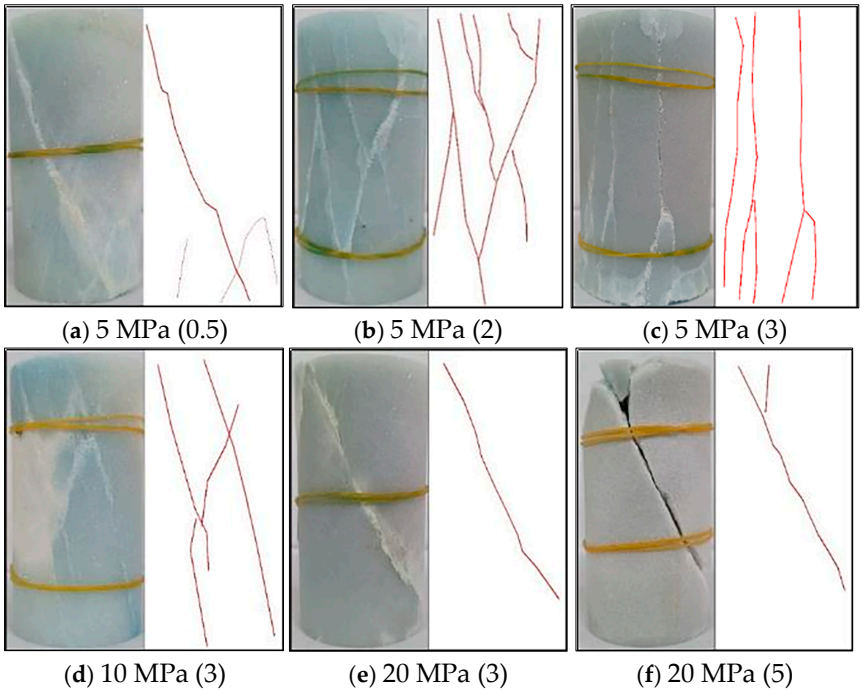


Figure 12. Failure images of creep samples at various initial confining pressures.

Under conditions of low initial confining pressure and small unloading amount, the specimen mainly exhibits a single oblique shear main crack, accompanied by a small number of tensile secondary cracks. As the unloading amount increases, the number of tensile–shear cracks significantly increases, and the crack inclination angle gradually increases.

Under conditions of high initial confining pressure and small unloading amount, the specimen mainly undergoes shear failure, and the confining pressure has a stabilizing constraint effect on the expansion of the shear zone. However, under conditions of high initial confining pressure and large unloading amount, the specimen exhibits typical "X" type tensile–shear composite cracks, indicating that the shear failure and tensile failure jointly play a dominant role in the instability process.

4. Construction and Verification of the Creep Constitutive Model

4.1. Model Construction

During the process of staged unloading of confining pressure and application of additional lateral pressure, marble exhibits attenuated creep, steady-state creep, and accelerated creep at different stress stages. The classic Nishihara model can effectively describe the first two stages, but cannot capture the nonlinear accelerated creep phase. To address this limitation, the non-stationary Nishihara creep model has been proposed in the literature by introducing a nonlinear viscoplastic element to replace the ideal viscoplastic element in the classical framework. In this study, we apply this model framework to the

specific stress path of stepwise confining pressure unloading with synchronous axial stress loading and validate its applicability to this path using experimental data. Although the non-stationary Nishihara model has been reported in the literature, its suitability for this complex excavation-induced path (progressive reduction in σ_3 with increasing deviatoric stress) has remained unexplored. By introducing stress- and time-dependent damage coefficients (α_0–α_3), the model accurately captures the accelerated creep characteristics of marble under this path, providing a validated tool for long-term stability analysis of deep surrounding rock. The schematic of the adapted mechanical model is shown in Figure 13.

$$\varepsilon = \frac{\sigma - \sigma_s}{\eta_2} t^n \tag{1}$$

where σ represents stress; ε represents strain; σ_s represents yield stress; and η_2 represents the nonlinear viscoplasticity coefficient of the material.

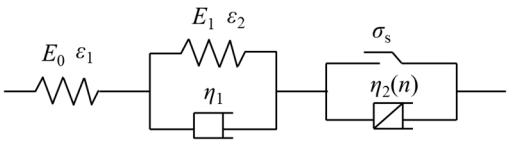


Figure 13. Non-stationary Nishihara mechanical model.

The model is composed of an elastic element, a viscoelastic element (generalized Kelvin unit) and a viscoplastic element, connected in series, where E_0 represents the elastic modulus of the elastic element; E_1 represents the elastic modulus in the Kelvin system; and η_1 represents the viscosity coefficient in the Kelvin system.

When $\sigma < \sigma_s$, the creep deformation of the Nishihara model is composed of instantaneous elastic deformation and viscoelastic deformation, respectively. By using the principle of superposition of the same instantaneous deformation [25], the creep equation of the Nishihara model is

$$\varepsilon = \varepsilon_1 + \varepsilon_2 = \frac{\sigma}{E_0} + \frac{\sigma}{E_1} + Ae^{-\frac{E_1}{\eta_1}t} \tag{2}$$

When $\sigma > \sigma_s$, the creep deformation of the Nishihara model needs to superimpose the deformation of the ideal viscoplastic element. At this time, the creep equation is obtained as

$$\varepsilon = \frac{\sigma}{E_0} + \frac{\sigma}{E_1}(1 - e^{-\frac{E_1}{\eta_1}t}) + \frac{\sigma - \sigma_s}{\eta_2} t \tag{3}$$

This equation can represent the trend of continuous increase in creep deformation as time progresses.

From Equations (1)–(3), the improved Nishihara model one-dimensional creep equation can be obtained as follows:

$$\begin{cases} \varepsilon = \frac{\sigma}{E_0} + \frac{\sigma}{E_1}(1 - e^{-\frac{E_1}{\eta_1}t}), & \sigma < \sigma_s \\ \varepsilon = \frac{\sigma}{E_0} + \frac{\sigma}{E_1}(1 - e^{-\frac{E_1}{\eta_1}t}) + \frac{\sigma - \sigma_s}{\eta_2} t^n, & \sigma \geq \sigma_s \end{cases} \tag{4}$$

Suppose there exists a variable D that can describe the aging damage of various mechanical parameters of rocks, and it is related to long-term strength and time. The following negative exponential function expression is obtained:

$$D = 1 - exp[-\alpha(\sigma - \sigma_\infty)t] \tag{5}$$

where α represents the damage influence coefficient; σ_∞ represents the long-term strength of the rock.

Assuming that the elastic modulus of the two elastic elements during the creep process is only related to the stress, and that of the two viscous elements is only related to time, then the damage variable D can be further simplified, and the following expression for the degradation of mechanical parameters due to damage can be obtained [26]:

$$\begin{cases} E_0(\sigma) = E_0 exp[-\alpha_0(\sigma - \sigma_\infty)] \\ E_1(\sigma) = E_1 exp[-\alpha_1(\sigma - \sigma_\infty)] \\ \eta_1(t) = \eta_1 exp(-\alpha_2 t) \\ \eta_2(t) = \eta_2 exp(-\alpha_3 t) \end{cases} \tag{6}$$

where α_0 and α_1 are the damage influence coefficients of the elastic elements. They quantify the degradation rate of the elastic moduli (E_0 and E_1) when the deviatoric stress (σ) exceeds the long-term strength (σ_∞). A higher α_0 or α_1 indicates a greater sensitivity of the material's elasticity to stress damage. α_2 and α_3 are the damage influence coefficients of the viscous elements. They represent the rate at which the viscous properties of the material deteriorate over time, reflecting the internal microstructural evolution that leads to accelerated flow.

In conclusion, the one-dimensional non-stationary Nishihara creep model can be obtained:

$$\varepsilon = \begin{cases} \frac{\sigma}{E_0 exp[-\alpha_0(\sigma-\sigma_\infty)]} + \frac{\sigma}{E_1 exp[-\alpha_0(\sigma-\sigma_\infty)]} \\ \cdot\left\{1 - exp\left[-\frac{E_1 exp[-\alpha_1(\sigma-\sigma_\infty)]}{\eta_1 exp(-\alpha_2 t)} t\right]\right\}, \ \sigma < \sigma_s \\ \frac{\sigma}{E_0 exp[-\alpha_0(\sigma-\sigma_\infty)]} + \frac{\sigma}{E_1 exp[-\alpha_0(\sigma-\sigma_\infty)]} \\ \cdot\left\{1 - exp\left[-\frac{E_1 exp[-\alpha_1(\sigma-\sigma_\infty)]}{\eta_1 exp(-\alpha_2 t)} t\right]\right\} + \frac{\sigma-\sigma_s}{\eta_2 exp(-\alpha_3 t)} t^n, \ \sigma \geq \sigma_s \end{cases} \tag{7}$$

In actual engineering projects, the rocks in underground engineering often undergo complex three-dimensional stress conditions. To accurately describe the creep deformation characteristics of the surrounding pressure in underground engineering, the one-dimensional creep model expressed by Formula (7) needs to be converted into a three-dimensional creep model. This experiment is a creep test under conventional triaxial conditions, so there is $\sigma_1 > \sigma_2 = \sigma_3$, and the non-stationary Nishihara creep model in three-dimensional state can be derived.

The creep model composed of the generalized Kelvin unit and the non-stationary viscoplastic element in series can be expressed as the axial total strain ε_{ij} in three-dimensional state as follows:

$$\varepsilon_{ij} = \varepsilon_{ij}^{e} + \varepsilon_{ij}^{\mathrm{ve}} + \varepsilon_{ij}^{\mathrm{vp}} \tag{8}$$

where ε_{ij}^{e}, ε_{ij}^{ve}, and ε_{ij}^{vp} represent the elastic deformation tensor, the viscoelastic deformation tensor, and the viscoplastic deformation tensor, respectively.

The stress tensor σ_{ij} and strain tensor ε_{ij} of the rock under triaxial loading conditions can be further decomposed as follows:

$$\begin{cases} \sigma_{ij} = S_{ij} + \delta_{ij}\sigma_m \\ \varepsilon_{ij} = e_{ij} + \delta_{ij}\varepsilon_m \end{cases} \tag{9}$$

where S_{ij} and σ_m represent the stress deviator tensor and the stress ellipsoid tensor, respectively; e_{ij} and ε_m represent the strain deviator tensor and the strain ellipsoid tensor, respectively; and δ_{ij} is the Kronecker tensor, which satisfies $\delta_{ij} = \begin{cases} 1, \ (i = j) \\ 0, \ (i \neq j) \end{cases}$.

When converting from one-dimensional to three-dimensional states, the volume modulus and shear modulus have the following relationship:

$$K = \frac{E_0}{2(1+\mu)}, G = \frac{E_0}{3(1-2\mu)} \tag{10}$$

where μ represents Poisson's ratio; K represents the volume modulus; and G represents the shear modulus.

From the generalized Hooke's law, the tensor form of the three-dimensional constitutive relationship for the elastic element is

$$\begin{cases} S_{ij} = 2Ge_{ij} \\ \sigma_m = 3K\varepsilon_m \end{cases} \tag{11}$$

Therefore, the formula for elastic strain in a three-dimensional stress state is

$$\varepsilon_{ij}^{e} = \frac{S_{ij}}{2G_0} + \frac{\delta_{ij}\sigma_m}{3K} \tag{12}$$

Under the conventional triaxial creep test, $\sigma_1 > \sigma_2 = \sigma_3$. Without considering the volume creep of three-dimensional state rocks, the strain formula for the elastic element can be known as

$$\varepsilon_{11}^{e} = \frac{\sigma_1 - \sigma_3}{3G_0\, exp[-\alpha_0(\sigma - \sigma_\infty)]} + \frac{\sigma_1 + 2\sigma_3}{9K\, exp[-\alpha_0(\sigma - \sigma_\infty)]} \tag{13}$$

where G_0 represents the shear modulus; G_0 represents the volume modulus.

Due to the parallel relationship, the strains of the elastic elements and viscous elements in Kelvin's model are equal. Assuming that the material damage influence coefficients α_1 and α_2 of the two are equal, the three-dimensional viscoelastic strain formula is

$$\varepsilon_{11}^{ve} = \frac{\sigma_1 - \sigma_3}{3G_1 exp[-\alpha_1(\sigma - \sigma_\infty)]}\left\{1 - exp\left(-\frac{G_1 exp[-\alpha_1(\sigma - \sigma_\infty)]}{\eta_1 exp(-\alpha_2 t)}t\right)\right\} \tag{14}$$

According to the generalized plasticity mechanics theory, the viscoplastic deformation of rocks cannot be directly replaced by the stress deviator tensor S_{ij} in the three-dimensional state with the stress σ in the one-dimensional state. It is related to the plastic potential function Q and the yield function F. According to the relevant flow law, the viscoplastic strain in the three-dimensional state is expressed as [27]

$$\varepsilon_{11}^{vp} = \frac{1}{\eta_2 exp[-\alpha_3 t]}\left[\Phi\left(\frac{F}{F_0}\right)\right]\frac{\partial Q}{\partial \sigma_{ij}}t^n \tag{15}$$

where $\left[\Phi\left(\frac{F}{F_0}\right)\right] = \begin{cases} 0, F < 0 \\ \Phi\left(\frac{F}{F_0}\right), F \geq 0 \end{cases}$, F is the yield function, F_0 is the initial value of the yield function, usually taken as 1, and Q is the plastic function, based on the flow rule $F = Q$.

Under normal temperature conditions, it is generally believed that the stress tensor has a relatively small influence on the creep deformation, while the stress components have a greater impact on the creep deformation. Therefore, the selected rock yield function is

$$F = \sqrt{J_2} - \frac{\sigma_s}{\sqrt{3}} = \frac{\sigma_1 - \sigma_3 - \sigma_s}{\sqrt{3}} \tag{16}$$

where J_2 represents the second invariant of the stress tensor.

In conclusion, the non-stationary axial creep model of rocks in three-dimensional state can be obtained as follows:

$$\varepsilon_{11}(t) = \begin{cases} \frac{\sigma_1-\sigma_3}{3G_0 exp[-\alpha_0(\sigma-\sigma_\infty)]} + \frac{\sigma_1+2\sigma_3}{9K exp[-\alpha_0(\sigma-\sigma_\infty)]} + \frac{\sigma_1-\sigma_3}{3G_1 exp[-\alpha_1(\sigma-\sigma_\infty)]} \\ \cdot\left\{1 - exp\left(-\frac{G_1 exp[-\alpha_1(\sigma-\sigma_\infty)]}{\eta_1 exp(-\alpha_2 t)}t\right)\right\}, \quad \sigma_1 - \sigma_3 < \sigma_s \\ \frac{\sigma_1-\sigma_3}{3G_0 exp[-\alpha_0(\sigma-\sigma_\infty)]} + \frac{\sigma_1+2\sigma_3}{9K exp[-\alpha_0(\sigma-\sigma_\infty)]} + \frac{\sigma_1-\sigma_3}{3G_1 exp[-\alpha_1(\sigma-\sigma_\infty)]} \\ \cdot\left\{1 - exp\left(-\frac{G_1 exp[-\alpha_1(\sigma-\sigma_\infty)]}{\eta_1 exp(-\alpha_2 t)}t\right)\right\} + \frac{\sigma_1-\sigma_3-\sigma_s}{\eta_2 exp(-\alpha_3 t)}t^n, \quad \sigma_1 - \sigma_3 \geq \sigma_s \end{cases} \tag{17}$$

In this model, 'non-stationary' refers to the incorporation of damage evolution into key mechanical parameters.

Elastic moduli (E_0, E_1) are treated as stress-dependent, degrading exponentially when the deviatoric stress exceeds the long-term strength (σ_∞), as described by damage coefficients α_0 and α_1 in Equation (6).

Viscosity coefficients (η_1, η_2) are treated as time-dependent, degrading exponentially with time as described by damage coefficients α_2 and α_3 in Equation (6).

4.2. Model Validation

4.2.1. Parameter Confirmation Method

In the three-dimensional non-stationary Nishihara model (Formula (17)), the two parameters, the initial volume modulus K and the initial shear modulus G_0, can be determined by the following method.

Assuming that all instantaneous deformations are elastic deformations, the initial volume modulus K of the rock is

$$K = \frac{\sigma_m}{3\varepsilon_m} = \frac{\sigma_m}{\varepsilon_v} \tag{18}$$

The initial shear modulus G_0 is

$$G_0 = \frac{3KS_{ij}}{6K\varepsilon_0 - 2\sigma_m} \tag{19}$$

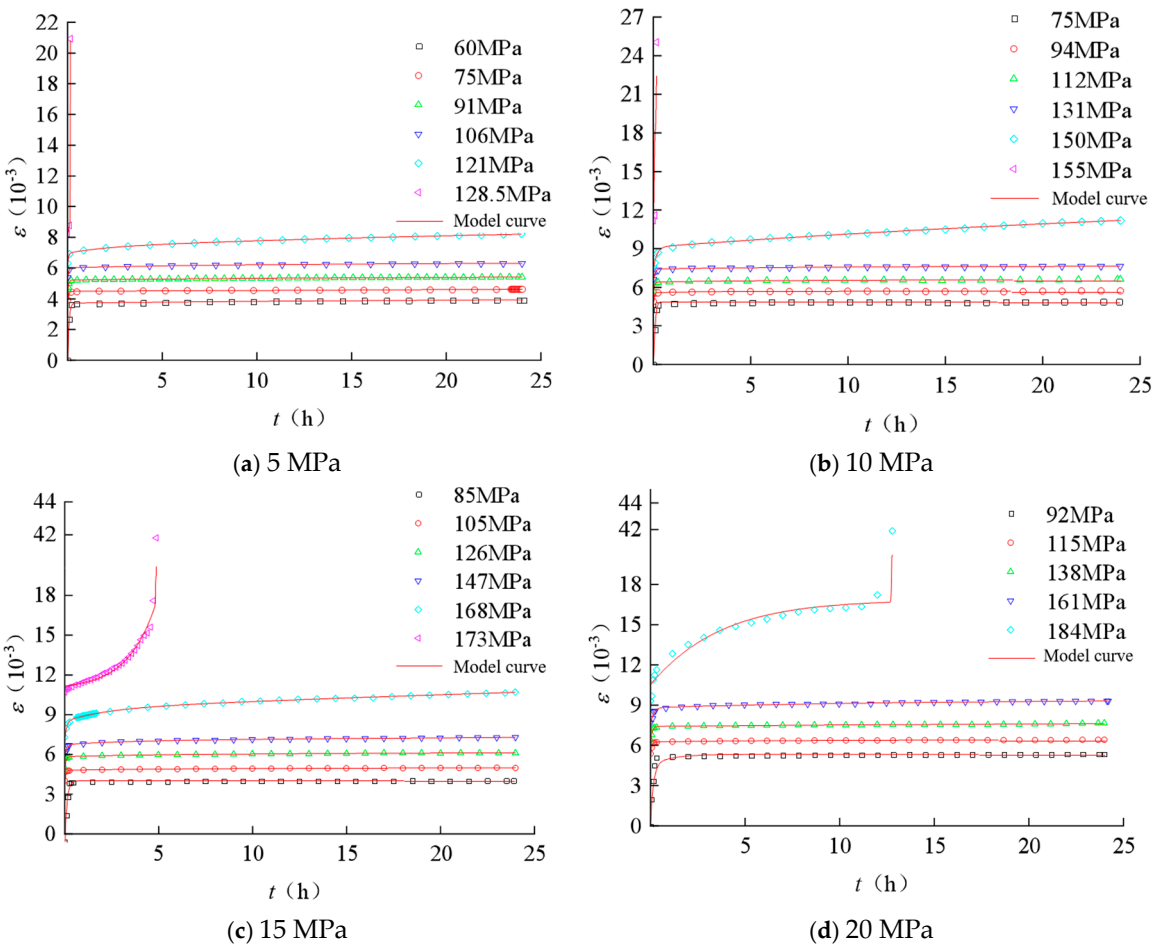
where ε_0 represents the instantaneous elastic strain.

The other nine parameters G_1, α_0, α_1, α_2, α_3, η_1, η_2, σ_∞ and n of the three-dimensional non-stationary Nishihara creep model can be obtained through the curve fitting toolbox of MATLAB R2017a.

4.2.2. Validation Results and Comparison

Samples with initial confining pressures of 5, 10, 15, and 20 MPa were taken, and the creep test curves under staged confining pressure reduction and loading were analyzed. The comparison of the model calculation results with the experimental results is shown in Figure 14.

The results show that the non-stationary Nishihara creep model can well describe the entire process of attenuation creep, steady-state creep and accelerated creep of marble under different stress conditions. The goodness-of-fit R^2 of the model is all greater than 0.85, indicating high reliability.



(**a**) 5 MPa (**b**) 10 MPa

(**c**) 15 MPa (**d**) 20 MPa

Figure 14. Comparison between test data and model curve.

5. Conclusions

(1) Under the path of unloading confining pressure and deviatoric stress, the creep process of marble can be divided into three stages: attenuation creep, steady creep, and acceleration creep. As shown in Figures 3 and 4, with increasing confining pressure unloading magnitude, the creep failure stress decreases significantly, and the total test duration is markedly shortened. This indicates that unloading of confining pressure is a key factor controlling the long-term stability of marble.

(2) The creep rate analysis (Figure 5) shows that under small unloading conditions, the creep rate initially decreases and then increases with stress level; under large unloading conditions, it increases monotonically. This reflects that confining pressure unloading significantly weakens the stability of the rock mass during creep, with larger unloading steps accelerating failure.

(3) The long-term strength of marble was determined using the isochronous stress–strain curve method (Table 2). As initial confining pressure increases and unloading magnitude increases, the ratio of long-term strength to failure strength generally decreases (ranging from 0.86 under uniaxial conditions to 0.73–0.80 under unloading conditions), reflecting the reduction in the time-dependent strength margin under unloading conditions.

(4) Based on the graded unloading creep test results, a three-dimensional non-stationary Nishihara creep model was validated for the specific stress path of stepwise confining pressure unloading with synchronous axial stress loading. The model effectively captures the full creep process of marble under this path. From an engineering perspective, it provides a theoretical basis for predicting long-term convergence deformation in

deep excavations. By incorporating in situ stress fields and excavation sequences, the model can help estimate optimal timing for secondary lining installation and assess long-term tunnel serviceability, offering a quantitative tool for design and safety assessment in similar rock masses.

Author Contributions: Conceptualization, Z.Y., S.W. and Y.G.; data analysis, Z.Y. and S.W.; methodology, Z.Y.; software, S.W.; supervision, Y.G.; writing—original draft preparation, Z.Y.; writing—review and editing, J.L., H.D. and Y.G. All authors have read and agreed to the published version of the manuscript.

Funding: This research was funded by the National Natural Science Foundation of China (Grant No. 51439003, U22A20600).

Institutional Review Board Statement: Not applicable.

Informed Consent Statement: Not applicable.

Data Availability Statement: The original contributions presented in this study are included in this article; further inquiries can be directed to the author.

Acknowledgments: The authors acknowledge all the participants and administrators in this study.

Conflicts of Interest: The authors declare that this research was conducted in the absence of any commercial or financial relationships that could be construed as potential conflicts of interest.

References

1. Xiong, Z.; Lu, H.; Wang, M.; Qian, Q.; Rong, X. Research progress on safety risk management of large-scale geotechnical engineering construction in China. *Rock Soil Mech.* **2018**, *39*, 3703–3716.
2. Yang, C.; Wang, G.; Wang, J.; Yin, L.; Mao, H. Study on rock mechanics and seepage characteristics of Beishan preselected area in Gansu. *Rock Mech. Eng.* **2006**, *25*, 825–832.
3. Wang, M.; Zhou, Z.; Qian, Q. Structure, deformation and failure of deep rock mass. *J. Rock Mech. Eng.* **2006**, *25*, 448–455.
4. Su, Y. Fractional creep constitutive model of rock considering time-dependent damage. *J. Yangtze River Sci. Res. Inst.* **2022**, *39*, 92–97.
5. Gao, Y.; Zhou, H.; Zhang, C.; Chen, J.; He, S.; Liu, N. Theoretical study on aging strength of hard brittle rock. *J. Rock Mech. Eng.* **2018**, *37*, 671–678.
6. Huang, B.; Zhang, N.; Jing, H.; Kan, J.; Meng, B.; Li, N.; Xie, W.; Jiao, J. Theory of peripheral rock rheology and large deformation of structural instability in deep well mining roadways. *J. Coal* **2020**, *45*, 911–926.
7. Hadiseh, M.; Rassoul, A. Mechanical behavior of salt rock under uniaxial compression and creep tests. *Int. J. Rock Mech. Min. Sci.* **2018**, *110*, 19–27.
8. Zhang, J.; Yang, Z.; Du, R.; Xiang, X.; Chen, Y. Research on the Deformation Characteristics of Tunnel Structures Based on Anisotropic Creep Properties. *Chin. J. Undergr. Space Eng.* **2025**, *21*, 917–928.
9. Mohammadreza, A.; Hossein, M.; Amin, H.P.; Leandro, R.A. Estimating time-to-failure and long-term strength of rocks based on creep strain rate model. *Rock Mech. Rock Eng.* **2025**, *58*, 4207–4223.
10. Zhao, Y.; Niu, X.; Qi, X.; Hua, Y. Creep Long-Term Strength of Marble Under Coupling Effect of Hydration Freezing-Thaw. *J. Jilin Univ. (Earth Sci. Ed.)* **2025**, *55*, 188–198.
11. Mishra, B.; Verma, P. Uniaxial and triaxial single and multistage creep tests on coal-measure shale rocks. *Int. J. Coal Geol.* **2015**, *137*, 55–65. [CrossRef]
12. Zhao, N.; Zhang, Y.B.; Wang, L. Experimental study on multi-scale evolution of creep rupture of sandstone. *J. Appl. Mech.* **2023**, *40*, 87–95.
13. Li, Z.; Zhou, J.; Zhang, D.; Zhang, L.; Zeng, Q.; Yang, Z.; Fu, Y. Experimental study on the influence of dry-wet cycle on creep characteristics of argillaceous siltstone in longyou grottoes. *J. Eng. Geol.* **2024**, *32*, 2003–2016.
14. Guo, Y.; Wang, S.; Li, J.; Hu, P.; Wang, X. Creep Characteristics of Saturated Sandstone under Different Water Pressures by Stepwise Loading. *Chin. J. Undergr. Space Eng.* **2025**, *21*, 910–916.
15. Hu, M.; Xiao, B.; Lu, Y.; Zhang, Y.; Zhang, Y. Creep tests and creep model for reconstituted over-consolidated saturated clay. *Chin. J. Geotech. Eng.* **2023**, *45*, 6–10.
16. Shi, W.; Xu, X.; Huang, T.; Xiang, L.; Lei, X. Unloading creep test and long-term strength of soft rock under different initial stresses. *Sci. Technol. Eng.* **2022**, *22*, 11577–11584.

17. Zhou, R.; Cheng, H.; Cai, H.; Liu, T. Creep characteristics and creep modeling of siltstone under triaxial compression and graded unloading conditions. *J. Rock Mech. Eng.* **2022**, *41*, 1136–1147.
18. Yan, Z.; Xia, C.; Li, H. Study on rheological law of Jinping marble under graded unloading conditions. *Chin. J. Rock Mech. Eng.* **2008**, *27*, 2153–2159.
19. Ni, J.; Li, S.; Hang, Y.; Wei, Y. Experimental study on creep behavior of saturated soft clays under loading and unloading conditions. *J. Eng. Geol.* **2019**, *27*, 1262–1269.
20. Liu, X.; Li, S.; Zhou, Y.; Li, Y.; Wang, W. Study on creep properties and long-term strength of high-stress muddy siltstone. *J. Rock Mech. Eng.* **2020**, *39*, 138–146.
21. Guo, X.; Li, W. Mechanical Properties and Damage Analysis of Cyclic Freeze-thaw Creep of Saturated Rock. *Sci. Technol. Eng.* **2024**, *24*, 7584–7591.
22. *GB/T 50266-2013*; Standard for Test Methods of Engineering Rock Mass. Ministry of Housing and Urban-Rural Development of the People's Republic of China: Beijing, China, 2013.
23. Qian, Y.; Wu, Y.; Pei, W.; Zhu, Y. Strength and deformation characteristics of rock under different unloading rates. *J. Water Conserv. Water Transp. Eng.* **2020**, 48–54. [CrossRef]
24. Zhou, J.; Jing, M.; Fan, C.; Wang, J. Method for determining the long-term strength of Jinping marble under true triaxial stress. *Chin. J. Rock Mech. Eng.* **2023**, *42*, 3324–3330.
25. Wang, Z.; Li, Y. *Rock Mass Rheology Theory and Its Numerical Simulation*; Science Press: Beijing, China, 2008; pp. 7–27.
26. Zhang, X.; Lin, H.; Wang, Y.; Zhao, Y. Creep damage model of rock mass under multi-level creep load based on spatio-temporal evolution of deformation modulus. *Arch. Civ. Mech. Eng.* **2021**, *21*, 71. [CrossRef]
27. Guan, S.; Wang, L.; Sun, C. Rock fractional order statistical damage rheological constitutive model. *J. Liaoning Tech. Univ. (Nat. Sci. Ed.)* **2021**, *40*, 518–524.

Disclaimer/Publisher's Note: The statements, opinions and data contained in all publications are solely those of the individual author(s) and contributor(s) and not of MDPI and/or the editor(s). MDPI and/or the editor(s) disclaim responsibility for any injury to people or property resulting from any ideas, methods, instructions or products referred to in the content.